Web of Science Group Master Journal Lists   Match Manuscript   Downloads   Help Center   Login

Already have a manuscript?

Use our Manuscript Matcher to find the best relevant journals!

Find a Match

Refine Your Search Results

2187-0764   Search

Sort By: Title (A-Z)   ▼

Search Results

Found 1 results (Page 1)   ⤳ Share These Results

Filters   🗑 Clear All

Web of Science Coverage   ⌄

Open Access 🔓   ⌄

Category   ⌄

Country / Region   ⌄

Language   ⌄

Frequency   ⌄

Journal Citation Reports   ⌄

Exact Match Found

JOURNAL OF ASIAN CERAMIC SOCIETIES

OPEN ACCESS

Publisher:	TAYLOR & FRANCIS LTD , 2-4 PARK SQUARE, MILTON PARK, ABINGDON, England, OXON, OX14 4RN
ISSN / eISSN:	2187-0764
Web of Science Core Collection:	Science Citation Index Expanded
Additional *Web of Science* Indexes:	Current Contents Engineering, Computing & Technology | Current Contents Physical, Chemical & Earth Sciences | Essential Science Indicators

⤳ Share This Journal

View profile page

Requires free login.

Taylor & Francis Online

Login | Register | Cart

Home ▸ All Journals ▸ Journal of Asian Ceramic Societies ▸ List of Issues ▸ Volume 6, Issue 4 ▸ Morphological and photoluminescence stud ...

Enter keywords, authors, DOI, ORCID etc   This Journal
Advanced search

Submit an article   Journal homepage

◀ Listen ▶

Morphological and photoluminescence study of $NaSrB_5O_9$: Tb^{3+} nanocrystalline phosphor

Vaishali Raikwar ✉ ⓘ, Vinod Bhatkar & Shreeniwas Omanwar

❝ Download citation   ☑ https://doi.org/10.1080/21870764.2018.1529014   ⓡ Check for updates

▸ Full Article   ☑ Figures & data   ☷ References   ❝ Citations   ☷ Metrics   ⓒ Licensing   ☷ Reprints & Permissions   ☷ PDF

ABSTRACT

Nanocrystalline green-emitting phosphor $NaSrB_5O_9$: Tb^{3+} was synthesized by a facile and time-efficient modified combustion method. The phosphor was characterized by powder X-ray diffraction (XRD), Fourier transform infrared (FTIR) spectroscopy, nanoparticle tracking analysis (NTA), field emission scanning electron microscopy (FESEM) and photoluminescence excitation (PLE) and emission (PL) spectroscopy. XRD revealed the proper phase formation. Williamson–Hall (W-H) analysis gave the crystallite sizes and lattice strain due to peak broadening. A nanoplate-like morphology was observed in the FESEM analysis. Upon excitation by 217 nm UV light, the phosphor showed characteristic green emission peaks at 487 nm, 543 nm, 596 nm and 622 nm corresponding to the $^5D_3 \rightarrow {}^7F_5$, $^5D_3 \rightarrow {}^7F_3$, $^5D_4 \rightarrow {}^7F_4$ and $^5D_4 \rightarrow {}^7F_3$ transitions, respectively. A concentration quenching effect was observed and the critical concentration was found to be 3 mol % of Terbium.

Q KEYWORDS: $NaSrB_5O_9$: Tb^{3+} green emission   modified combustion method   nanoplate-like morphology

In this article

ABSTRACT

1. Introduction

2. Experimental

3. Results and discussion

4. Conclusion

Disclosure statement

References

Morphological and photoluminescence study of NaSrB$_5$O$_9$: Tb^{3+} nanocrystalline phosphor

Vaishali Raikwar, Vinod Bhatkar & Shreeniwas Omanwar

Submit your article to this journal ☑

View Crossmark data ☑

Certified as
TRUE COPY

Principal
Ramniranjan Jhunjhunwala College,
Ghatkopar (W), Mumbai-400086.

THE CERAMIC SOCIETY OF JAPAN   THE KOREAN CERAMIC SOCIETY   Taylor & Francis
Taylor & Francis Group

FULL LENGTH ARTICLE   ∂ OPEN ACCESS   Check for updates

Morphological and photoluminescence study of NaSrB$_5$O$_9$: Tb^{3+} nanocrystalline phosphor

Vaishali Raikwar [ORCID][a], Vinod Bhatkar[b] and Shreeniwas Omanwar[c]

[a]Department of Physics, R. J. College, Mumbai, India; [b]Department of Physics, Shri Shivaji Science College, Amravati, India; [c]Department of Physics, SGB Amravati University, Amravati, India

ABSTRACT

Nanocrystalline green-emitting phosphor NaSrB$_5$O$_9$: Tb^{3+} was synthesized by a facile and time-efficient modified combustion method. The phosphor was characterized by powder X-ray diffraction (XRD), Fourier transform infrared (FTIR) spectroscopy, nanoparticle tracking analysis (NTA), field emission scanning electron microscopy (FESEM) and photoluminescence excitation (PLE) and emission (PL) spectroscopy. XRD revealed the proper phase formation. Williamson–Hall (W-H) analysis gave the crystallite sizes and lattice strain due to peak broadening. A nanoplate-like morphology was observed in the FESEM analysis. Upon excitation by 217 nm UV light, the phosphor showed characteristic green emission peaks at 487 nm, 543 nm, 596 nm and 622 nm corresponding to the $^5D_4 \rightarrow {}^7F_6$, $^5D_4 \rightarrow {}^7F_5$, $^5D_4 \rightarrow {}^7F_4$ and $^5D_4 \rightarrow {}^7F_3$ transitions, respectively. A concentration quenching effect was observed and the critical concentration was found to be 3 mol % of Terbium.

1. Introduction

In this era of advanced technologies, nanoscale materials have become an unavoidable part of the equipment in almost every field. In fact, the many positive developments/inventions using nanomaterials so far have triggered a need for developing more and more nanomaterials and exploring the opportunities in myriad fields that can contribute to making life better. For the past three decades, luminescent materials doped with rare earth ions have been studied and developed globally for possible applications in fields such as medical diagnosis, displays, optical communication systems, mobile phone screens, general lighting equipment such as tricolor lamps and white light emitting diodes (WLEDs) [1–5]. Inorganic borates doped with rare earth ions have found an important place in various research fields, moreover, due to their high optical applications, varied structural types, low synthesis temperatures, high chemical and thermal stability, and low cost and high luminescence efficiency. Many alkaline earth metal borates are reported for UV emissions used in medical applications [6] and various other applications [7–12]. They have a large band gap and covalent band energy. Alkaline earth metal borates doped with terbium are developed mainly due to their superior color purity, low synthesis temperature, and good mechanical and electrical properties. Among the alkaline earth borates NaSrB$_5$O$_9$ has not been studied much. A NaSrB$_5$O$_9$ crystal structure was first reported by Wu et al. in 2007 [13]. Because of their similar radii, the Sr^{2+} ions in NaSrB$_5$O$_9$ can be easily replaced by rare earth

ions for developing phosphors, which are light-emitting materials. Until recently, reports have concerned NaSrB$_5$O$_9$:Dy^{3+}, NaSrB$_5$O$_9$:Eu^{3+} and NaSrB$_5$O$_9$:Sm^{3+} achieved by the conventional solid-state reaction method with prolonged heating of 8 h at 800°C [14–16]. The solid-state method is carried out at relatively high temperatures, however, requires long annealing period after synthesis. It also requires intermittent grinding and washing which can, in turn, add impurities to the products. A soft chemical method such as combustion, on the other hand, does not require high temperatures for the synthesis. It requires only a simple setup and takes considerably less time for processing. This method is carried out at relatively low temperature and requires no absolute control over the synthesis temperature. The oxidizer and fuel ratio automatically decide the temperature during synthesis [17]. The same technique is used efficiently for synthesis of aluminate [18–20], borate [21–24], silicate [25–27] and phosphate phosphors [28]. We report here the synthesis and photoluminescence properties of NaSrB$_5$O$_9$:Tb^{3+} achieved using a facile, time-efficient and economical method of modified combustion with urea as fuel for the first time. The reported phosphor shows uniform morphology with the good emission intensity required for purposes of practical application in optical devices.

2. Experimental

NaSr$_{1-x}$B$_5$O$_9$:xTb^{3+} phosphors doped with various molar concentrations of Tb^{3+} (x = 0.005, 0.01, 0.02,

Certified as
TRUE COPY

Principal
Ramniranjan Jhunjhunwala College,
Ghatkopar (W)   ubai-400086.

0.03, 0.05) were prepared by a modified combustion technique. The synthesis is based on an exothermic reaction between the fuel and oxidizer. Urea was used as the fuel and metal nitrates as the oxidizer. For complete combustion the oxidizer-to-fuel ratio should be one-to-one. All the precursors viz. sodium nitrate, strontium nitrate, urea and boric acid (as the boron source) were procured as analytical reagents (AR), weighed in stoichiometric proportions and dissolved in a minimum amount of distilled water. Terbium nitrate was prepared by adding dilute HNO_3 to terbium oxide followed by continuous stirring. The precursor paste was mixed well to assure homogenization of the mass. A quartz container containing this paste was placed in a furnace maintained at around 550°C. After about 2–3 min a reaction with bright yellow flames started. The reaction continued for only a few seconds. As soon as the reaction was over, the quartz container was removed from the furnace and allowed to cool. The prepared phosphor was crushed to a fine powder using a mortar and pestle. The same process flow was followed for the different concentrations of Tb^{3+}. The samples were subjected to X-ray diffraction (XRD) analysis using a Rigaku Miniflex diffractometer with Cu Kα radiation (λ = 1.54059 A°) operating at 40 kV and 30 mA. The XRD data was collected in the 2θ range from 10° to 70° at room temperature. Fourier transform infrared (FTIR) spectroscopy was conducted on a Shimatzu IR Prestige −21 analyser. The measurements concerning particle size were done with a nanoparticle tracking analysis (NTA) system that uses a laser to track the Brownian motion of particles in samples. The measurements of photoluminescence emission (PL) over the range of 450 to 650 nm and photoluminescence excitation spectra (PLE) over a 200 to 400 nm excitation range were conducted with a Hitachi F 7000 fluorescence spectrophotometer at room temperature. The

spectral resolution of both the excitation and emission spectra widths of the monochromatic slits (1 nm) as well as of measurement conditions such as the photomultiplier tube detector's sensitivity and scanning speed were kept constant for all the samples. Electron diffraction X-ray spectroscopy (EDX) for elemental analysis and field emission scanning electron microscopy (FESEM) for detecting the morphology of the samples was conducted on a Hitachi S-4800 FESEM with a maximum resolution of 1.0 nm and a variable acceleration voltage of 0.5–30 kV. All the samples were coated with a thin layer of gold in the FESEM analysis to avoid charging. The color chromaticity coordinates were obtained following the standards of the Commission International de l'Eclairage (CIE) using Radiant Imaging Color Calculator 2.0 software.

3. Results and discussion

3.1. XRD analysis

Figure 1 presents the powder XRD pattern of $NaSrB_5O_9$ prepared by the combustion method, which is in good agreement with the XRD data for $NaSrB_5O_9$ reported by Wu et al.in 2007 [13]. The consistent results for different dopant concentrations indicate that a single phase polycrystalline $NaSrB_5O_9$ was obtained by the combustion method in this study. According to Wu et al. $NaSrB_5O_9$ crystallizes in a monoclinic phase with space groups of $P2_1/c$. The crystal parameters are a = 6.4963 (1) A°, b = 13.9703(2) A°, c = 8.0515 (1) A°, β = 106.900 (1), volume = 699.16 (2)$A^{°3}$, Z = 4, density d = 2.93 g/cm^3.

The fundamental building unit of $NaSrB_5O_9$ is the $[B_5O_9]^{3-}$ anionic group, which is composed of three $[BO_3]$ triangles. It is composed of separated $[B_5O_9]^{3-}$

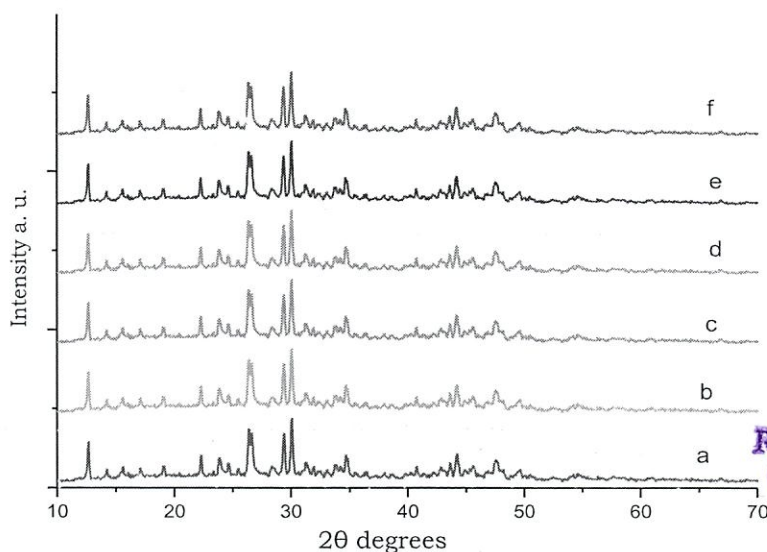**Figure 1.** XRD pattern for $NaSrB_5O_9$ (a) undoped and (b) – (f) doped with (0.5, 1, 2, 3, 5) mol % of Tb^{3+}, respectively.

anionic sheets, with [NaO$_8$] polyhedra acting as the connections between the sheets. The Sr atoms are located in the anionic sheets and surrounded by [BO] groups [13].

Calculation of the percentage difference between the ionic radii of doped and host matrices gives a clear picture of site occupancy by dopant ions. The acceptable percentage difference between the ionic radii of doped ions and substituting ions should not exceed 30 % [29]. The calculations of the radius percentage differences (Dr) between the doped ions (Tb^{3+}) and possible substituting ions (Na, Sr, B) in NaSrB$_5$O$_9$:Tb^{3+} are summarized in Table 1. The values are calculated according to the formula:

$$Dr = \frac{Rm(CN) - Rd(CN)}{Rm(CN)} \qquad (1)$$

where R$_m$ is the radius of host cations, R$_d$ is the radius of the dopant ions, and CN is the coordination number. Thus, it is clear that the Tb^{3+} ionic radius (r = 1.18 A°, CN = 8) is closest to that of Sr^{3+}(r = 1.26 A°, CN = 8), making it unlikely that Tb^{3+} would substitute for Na$^+$(r = 1.02 A°, CN = 6) or B^{3+}(r = 0.11, CN = 3) in the NaSrB$_5$O$_9$ host. Hence, it is believed that Tb^{3+} replaces the Sr^{2+} site in the NaSrB$_5$O$_9$ host.

XRD peak broadening originates from various factors, such as crystallite size, lattice strain and instrumental configuration. The peak properties can be analyzed by different methods, including the simplified integral breadth method, Fourier method and double Voigt method. The most commonly used method for calculating crystallite size from the XRD peak broadening is a simplified expression obtained by Scherrer [30,31], as follows:

$$T = \frac{0.9\lambda}{B \cos\theta} \qquad (2)$$

where T is the crystallite size of the scattering particles in nm, λ is the x-ray wavelength in nm, and B (in radians) is the full width at half maximum (FWHM) of one of the fundamental peaks scattered at an angle of θ. The crystallite size calculated by the Scherrer formula was found to be 35 nm. The Scherrer equation does not take into consideration the lattice strain factor in calculating the crystallite size. The Williamson–Hall (W–H) method is a more accurate method of calculating lattice strain and

crystallite size which is conducted according to following equation:

$$\beta r \cos \theta = \frac{K\lambda}{T} + 4\eta \sin \theta \qquad (3)$$

where βr is the total peak broadening, θ is the Bragg's angle and η is the strain distribution within the material [32–34]. $\beta_r \cos \theta$ is now plotted on the Y-axis and 4sin θ on the X-axis giving slope η and Y intercept Kλ/T. From the W–H plot, the Y- intercept can be obtained and used to calculate the crystallite size [Figure 2]. The grain size determined from W–H analysis is slightly higher than that calculated using Scherrer's formula. Table 2 summarizes the crystallite sizes calculated by Scherrer and W-H analysis and the strain calculated from W-H plots of NaSrB$_5$O$_9$ doped with various concentrations of Tb^{3+} ions. It is possible that the varying crystallite sizes may be due to the non-uniform strain generated in the crystal.

3.2. FTIR analysis

The representative FTIR spectra were recorded for two samples: NaSrB$_5$O$_9$ doped with 1 mol % and 3 mol %. As shown in Figure 3, the frequency modes were found to be same for molecules of NaSrB$_5$O$_9$ doped with the two concentrations. The bands between 450 cm^{-1} and 600 cm^{-1} are due to Na-O and Sr-O vibrations. The various sharp bands between 600 cm^{-1} and 824 cm^{-1} are due to overlapping BO$_3$ and BO$_4$ bending modes. The asym-
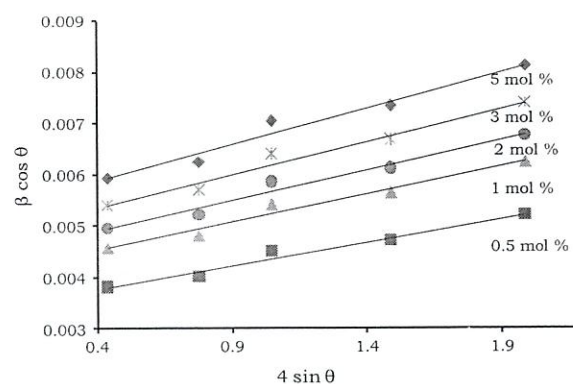

Figure 2. W-H plots for NaSrB$_5$O$_9$ doped with (0.5, 1, 2, 3, 5) mol % of Tb^{3+}.

Table 1. Ionic radii percentage differences between matrix and doping ions.

Ions in the matrix	Ionic radius r (A°)	CN	Dr
Tb^{3+}	1.18	8	–
Sr^{2+}	1.26	8	6.35 %
Na$^+$	1.02	6	−13.56 %
B^{3+}	0.11	3	−972.73 %

Table 2. Crystallite size and strains of NaSrB$_5$O$_9$ doped with (0.5, 1, 2, 3, 5) mol % of Tb^{3+}.

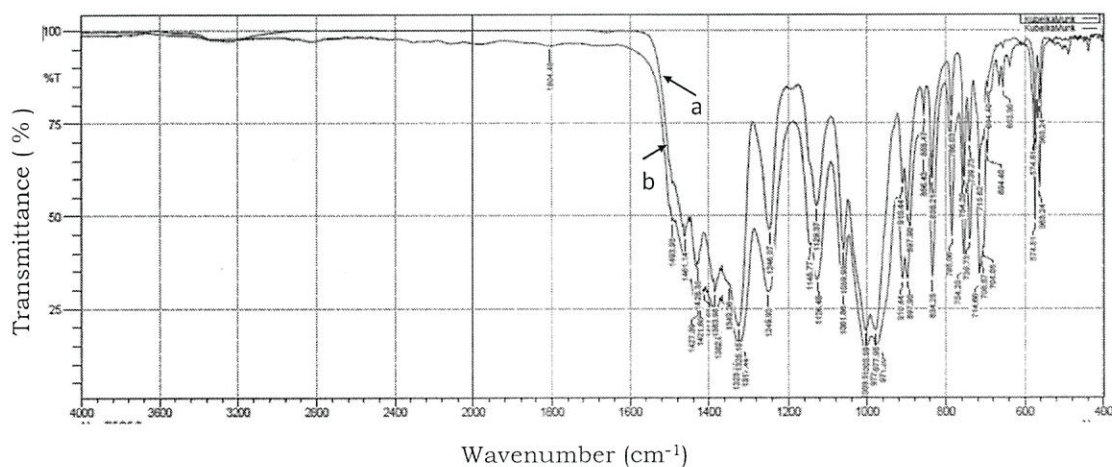| NaSrB$_5$O$_9$: Tb^{3+}(mol %)	Crystallite size (nm)		Lattice strain η (X 10^{-3})
	Scherrer Equation	W-H analysis	
0.5	28	27.72	1.12
1	26	34.65	3.34
2	29	46.2	4.79
3	32	46.2	4.79
5	33	34.65	4.56

Figure 3. FTIR images of NaSrB$_5$O$_9$ (a) doped with 1 mol % and (b) 3 mol % of Tb.

metric stretching modes of vibration of BO$_4$ cause bands between 965 cm^{-1} and 1020 cm^{-1}. Similarly the strong band at 1300 cm^{-1} is due to the stretching mode of the BO$_3$ group. A small band at around 3300 cm^{-1} is due to the presence of water content which arises due to the OH- group of water [35].

3.3. Nanoparticle tracking analysis (NTA)

NTA is a system for sizing particles from about 30 nm to 1000 nm where the lower detection limit is size-dependent on the refractive index of the nano-particles. This technique involves a combination of laser light-scattering microscopy and charge-coupled device (CCD) photography, which enables the visualization and recording of nanoparticles in solution. The corresponding software then identifies and tracks individual nanoparticles moving under Brownian motion. The movement of a particle is then related to a particle size according to a formula derived from the Stokes-Einstein Equation, as follows:

$$D_t = \frac{2TK_\beta}{3\pi\eta r_h} \tag{4}$$

where K$_\beta$ is the Boltzmann constant and Dt is the particle diffusion coefficient at room temperature T in a medium of viscosity η with a hydrodynamic radius of r$_h$ [36]. Thus, NTA converts the distances moved by the particles to a particle size and plots the accumulated results in real time as a particle size distribution profile. Figure 4 reveals the particle size distribution pattern and cumulative data for NaSrB$_5$O$_9$:Tb^{3+} phosphor with an optimized concentration of Tb^{3+} (3 mol %). The average size of
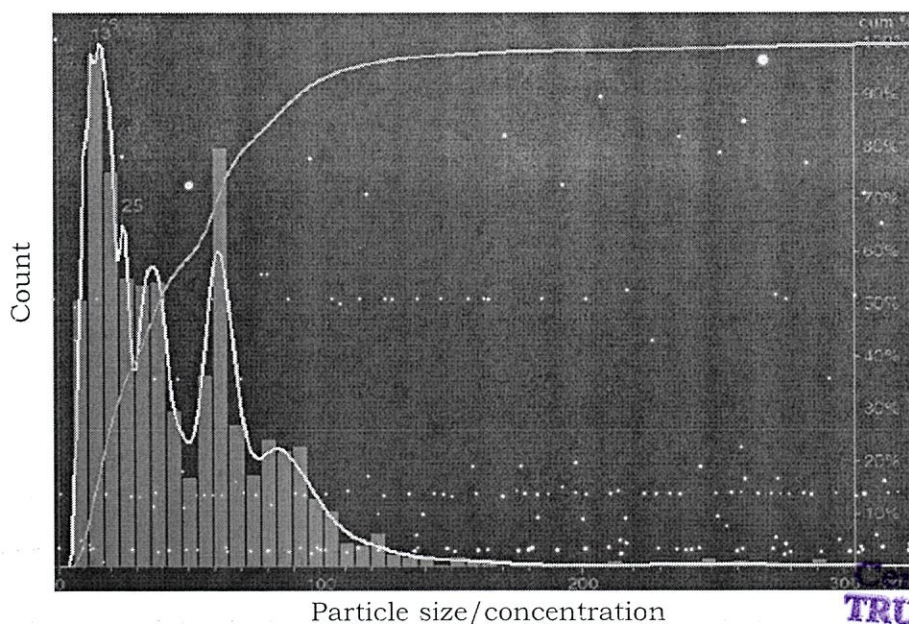

Figure 4. NTA particle size distribution of NaSrB$_5$O$_9$:Tb^{3+} phosphor for an optimized concentration of Tb^{3+} (3 mol %).

nanoparticles displayed in the distribution graph is approximately 36 nm.

3.4. FESEM analysis

Moreover, to study the effect of temperature on grain size, the sample is heated for 2 H at 650, 750 and 850° C. The crystallinity increases due to annealing, increasing the grain size. Figure 5 reveals this fact where the grain size of a sample annealed at 650°C is 675 ± 35 nm, that of a sample annealed at 750°C is 860 ± 25 nm and that of a sample annealed at 850°C is 900 ± 20 nm. It is worth noting that grains are made up of several agglomerated primary crystallites whose sizes are determined by XRD analysis. The reported phosphor has a plate-like morphology. The uniform plate-like structure is a result of the modified combustion synthesis method, which is advantageous over the conventional solid-state reaction method. The porous structure of the sample is attributed to a rapid combustion process and non-uniform distribution of the temperature and mass flow in the combustion flame created during an oxidation-reduction reaction that occurs in the process. The nanoparticles with sizes around 20–40 nm may form plate-like microstructures which are an obvious result of agglomeration of nano-particles. The morphology is a regularly arranged plate-like structure unlike the one reported earlier in an $NaSrB_5O_9$ host doped with Eu and Dy synthesized by the solid-state reaction method [14,15]. Hence, it can be shown that the modified combustion synthesis method is suitable to prepare $NaSrB_5O_9$ phosphors with uniform morphology.

To investigate the presence of Tb ions in the sample further, EDX spectroscopy was conducted for the optimized sample (Tb concentration 3 mol %). Figure 6 presents an EDX graph for $NaSrB_5O_9$:Tb^{3+} (3 mol %). Table 3 confirms the presence of Tb in the proper proportion and thereby confirms the purity of the sample.

3.5 Photoluminescence properties

A photoluminescence study was conducted for all the samples of $NaSrB_5O_9$ with various concentrations of Tb^{3+}. The PLE spectrum was monitored at 543 nm and exhibited peak at around 217 nm [Figure 7(a)] which was attributed to the charge transfer band Tb^{3+}-O^{2-}. PL spectra were monitored at 217 nm and contained several groups of sharp lines associated with $^5D_4 \rightarrow ^7F_J$ (J = 1–6) electronic transitions of the Tb^{+3} ion. Tb^{3+} ions absorb the excitation energy, and transitions from the ground state to the excited state (5d) occur, after which Tb^{3+} ions relax to the $^5D_4$ state. The $^5D_4$ state can be populated by one of two processes, a non-radiative multi-phonon relaxation from the 5d levels or a cross-relaxation involving the $^5D_3$-$^5D_4$ and $^7F_6$-$^7F_0$ transitions. The intense emission broad band has different peaks (from 400 nm to 650 nm) at 487, 543, 596 and 622 nm, with the maximum peak at 543 nm [Figure 7(b)]. Upon excitation by 217 nm UV light, the phosphor shows characteristic green emission peaks at 487, 543, 596 and 622 nm corresponding to the $^5D_4 \rightarrow ^7F_6$, $^5D_4 \rightarrow ^7F_5$, $^5D_4 \rightarrow ^7F_4$ and $^5D_4 \rightarrow ^7F_3$ transitions, respectively. The concentration quenching effect was observed, and the optimum concentration was found to be 3 mol % of Terbium.
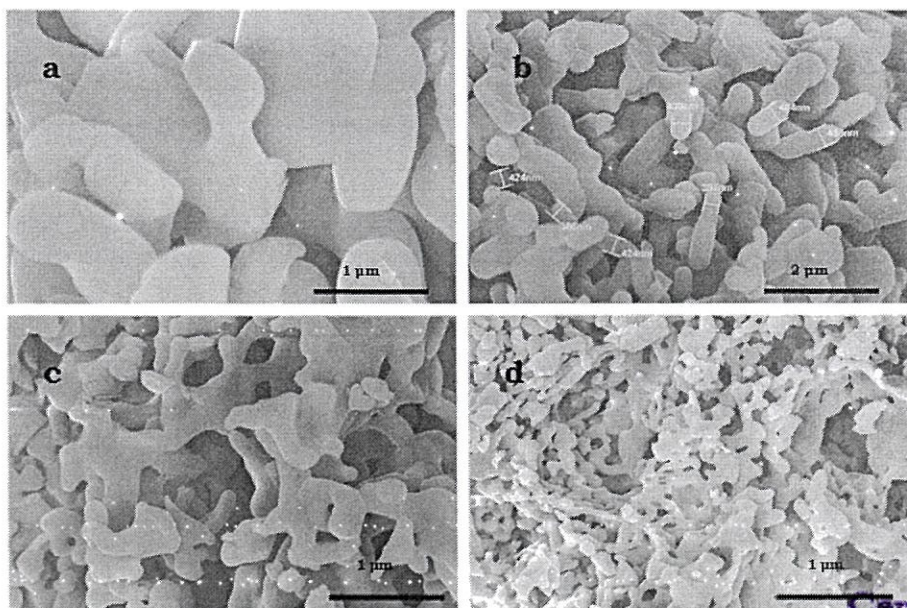

Figure 5. SEM micrographs of $NaSrB_5O_9$:Tb^{3+} annealed at different temperatures: (a) annealed at 850°C, (b) annealed at 750°C, (c) annealed at 650° C and (d) as prepared.
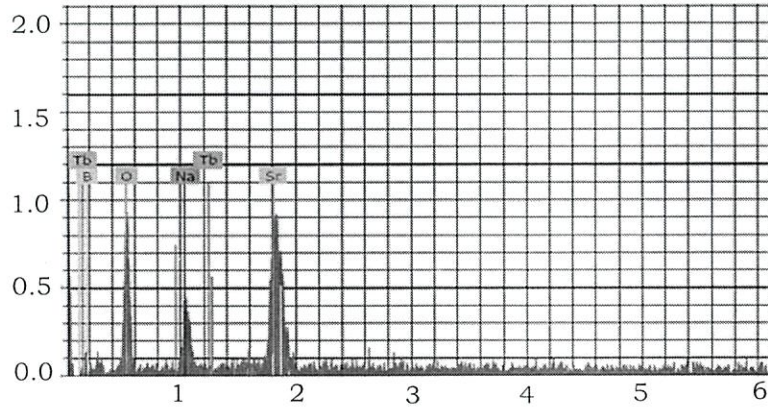
Figure 6. EDX graph of NaSrB$_5$O$_9$:Tb^{3+} phosphor for the optimum concentration of Tb^{3+} (3 mol %).

Table 3. EDX elemental analysis showing the precursors for NaSrB$_5$O$_9$:Tb^{3+} (3 mol %) with their weight %.

El	AN	Series	unn. C [wt %]	norm. C [wt %]	Atom. C[at %]
B	5	K-series	3.24	24.95	41.48
O	8	K-series	5.83	44.87	50.42
Na	11	K-series	0.45	3.43	2.68
Sr	38	L-series	3.41	26.25	5.39
Tb	65	L-series	0.03	0.30	0.03

In discussing the concentration quenching phenomenon, Blasse suggested that concentration quenching is generally associated with an energy transfer process from one activator ion to another (in this case the Tb^{3+} ion). The non-radiative energy transfer process has three causes: (i) exchange interaction, (ii) radiation reabsorption and (iii) multipolar interaction. If the activator is introduced solely on one crystallographic site (here the Sr^{2+} site), the critical energy transfer distance (Rc) is approximately equal to twice the radius of a sphere with this volume. In an NaSrB$_5$O$_9$ host, the critical energy transfer distance (Rc) can be calculated by the following equation:

$$Rc = 2\left(\frac{3V}{4\pi\,\chi c\,N}\right)^{1/3} \tag{5}$$

where χ_c is the critical concentration of doped ions, N is the number of cation sites in the unit cell and V is the volume of the unit cell. For NaSrB$_5$O$_9$, V = 699.16 A°, N = 4 and the critical concentration of Tb^{3+} in the NaSrB$_5$O$_9$ host is found to be 0.03. Hence the Rc of Tb^{3+} in NaSrB$_5$O$_9$: Tb^{3+} phosphor is determined to be 22.33 A°. Exchange interactions depend on a large direct or indirect overlap between the donor and acceptor, which is in turn responsible for the energy transfer of forbidden transitions and shorter critical distances of less than 5A° [37]. Since Rc is not less than 5 A°, exchange interactions are not responsible for non-radiative energy transfer
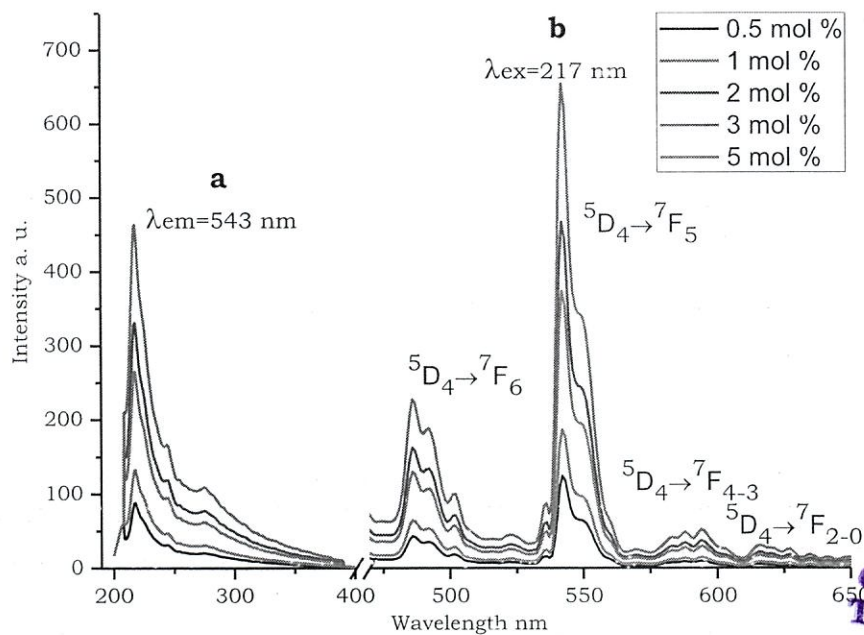

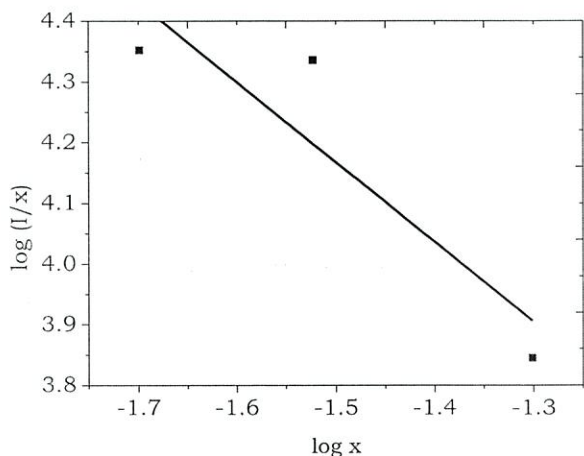**Figure 7.** Photoluminescence spectra of NaSr$_{1-x}$B$_5$O$_9$:xTb^{3+} phosphor (x = 0.05, 0.1, 0.2, 0.3, 0.5).

Figure 8. Plot of log (I/X) versus log x in NaSrB$_5$O$_9$:Tb^{3+} phosphor.

from one Tb^{3+} ion to another Tb^{3+} ion in this host. The second reason that quenching viz. the mechanism of radiation reabsorption is likely to occur is if the fluorescence spectra of the excitation and emission overlap. As there is no such overlap observed in NaSrB$_5$O$_9$: Tb^{3+} phosphor (Figure 6), radiation reabsorption is not a plausible reason for the concentration quenching. Thus, the energy transfer process of Tb^{3+} in NaSrB$_5$O$_9$: Tb^{3+} phosphor must be due to multipolar interaction.

To show that the energy transfer process occurs amongst the nearest ions, an empirical view of the relationship between emission intensity (I) and activator concentration (x) can be useful [38–40]:

$$\frac{I}{x} = \frac{K}{1 + \beta(x)^{\theta/3}} \qquad (6)$$

where k and β are constants for each interaction in a given host lattice. According to interaction theory, if θ = 3, the energy transfer occurs between nearest neighbor dopant ions; if θ = 6, 8 or 10 the energy transfer occurs due to a dipole-dipole, dipole-quadrupole or quadrupole-quadrupole interaction, respectively. The above relation can be solved further to get

$$\log\left(\frac{I}{x}\right) = K' - \frac{\theta}{3}\log x \qquad (7)$$

where K' = log K – log β. The optimal concentration of Tb^{3+} ions in this work is found to be 3 mol %. The graph of log (I/x) versus log x is plotted for 2, 3 and 5 mol % concentrations of Tb^{3+}, as shown in Figure 8. The graph is fitted for a straight line whose slope is (−θ/3) and from which θ is calculated. The value of θ is ≈3.94, which is close to 3. This indicates that the concentration quenching in this sample is the result of energy transfer between nearest neighbor Tb^{3+} dopant ions.

3.6. Color chromaticity

The color chromaticity coordinates are calculated for an optimal sample at 543 nm using Radiant Imaging Color Coordinates Calculator 2.0 software [41]. The observed values (0.254, 0.731) are very close to the Commission Internationale de'IEclairage (CIE) color coordinates for green color (0.288, 0.710). The calculated values are shown in the color chromaticity chart presented in Figure 9. The obtained color coordinates
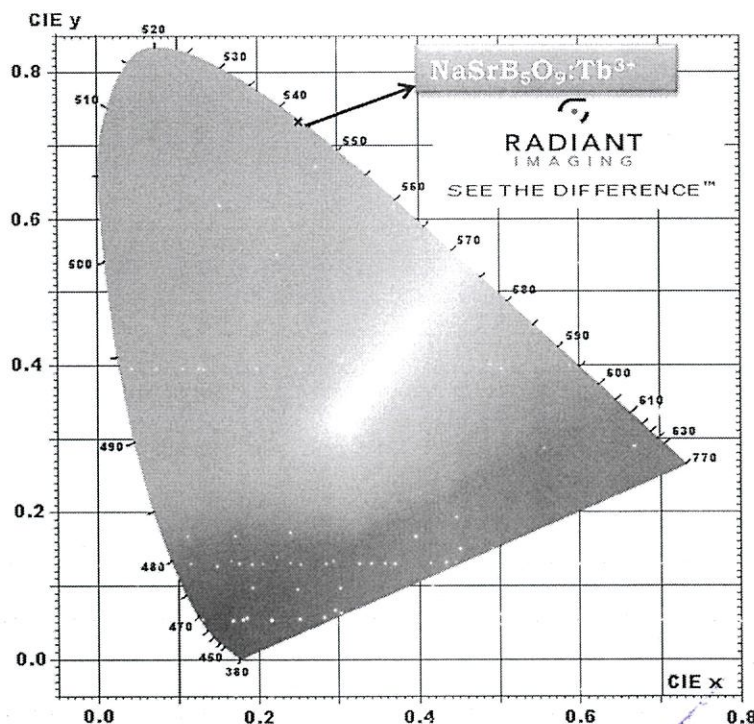

Figure 9. Color chromaticity chart for green-emitting NaSrB$_5$O$_9$:Tb^{3+}.

are located in the green region which indicates the feasibility of using the reported phosphor as a green-light-emitting phosphor for optical devices.

4. Conclusion

In conclusion, green color-emitting $NaSrB_5O_9:Tb^{3+}$ nanocrystalline phosphor was successfully prepared by modified combustion synthesis, and its structural and photoluminescent properties were studied. The nanocrystalline structure was confirmed by XRD analysis using the Scherrer formula and the W–H method of calculating crystallite size. NTA revealed the size distribution of the optimal sample when the particle size ≈36 nm. This proved that the combustion method is an effective method of producing nanocrystalline phosphor materials that can be useful in optical applications. The FESEM images showed an agglomeration of plate-shaped nanocrystallites. The photoluminescent emission spectrum showed intense green emission peaking at 487, 543, 596 and 622 nm corresponding to the characteristic Tb^{3+} transitions. The maximum intensity peak at 543 nm has CIE color coordinates (0.254, 0.731) which lie within the green chromaticity range on color chromaticity charts. The reported phosphor can thus be used in optical devices as a green color-emitting phosphor.

Highlights

- $NaSrB_5O_9$: Tb^{3+} nanocrystalline phosphor was synthesized for the first time by modified combustion synthesis at relatively low temperature.
- Nanoparticle tracking analysis (NTA) showed nanoparticles of average size ~ 36 nm.
- FESEM images showed a nanoplate-like morphology.
- Photoluminescence spectra showing green emissions revealed the feasibility of using this phosphor as a green light-emitting phosphor in optical devices.

Disclosure statement

No potential conflict of interest was reported by the authors.

ORCID

Vaishali Raikwar ⓘ http://orcid.org/0000-0002-2999-7065

References

[1] Gonda K, Watanabe M, Tada H, et al. Quantitative diagnostic imaging of cancer tissues by using phosphor-integrated dots with ultra-high brightness. Sci Rep. 2017;7(1):7509.

[2] Rong-Jun X, Naoto H, Takashi T. Wide color Gamut backlight for liquid crystal displays using three-band phosphor-converted white light-emitting diodes. Appl Phys Express. 2009;2(2):022401.

[3] Yiguang W, Yiguang W, Nan C, et al. Demonstration of 575-Mb/s downlink and 225-Mb/s uplink bi-directional SCM-WDM visible light communication using RGB LED and phosphor-based LED. Opt Express. 2013;21:1203–1208.

[4] Do YR, Bae JW. Application of photoluminescence phosphors to a phosphor-liquid crystal display. J Appl Phys. 2000;88:4660–4665.

[5] Gracia CR, Diaz-Torres LA, Oliva J, et al. Green $EuAlO_3:Eu^{2+}$ nanophosphor for applications in WLEDs. Opt Mater. 2014;37:520–524.

[6] Thakre DS, Omanwar SK, Muthal PL, et al. UV-emitting phosphors: synthesis, photoluminescence and applications. Phys Stat Sol. 2004;201(3):574–581.

[7] Peng M, Wondraczek L Orange-to-Red Emission from Bi^{2+} and Alkaline Earth Codoped Strontium Borate Phosphors for White Light Emitting Diodes. J Am Ceram Soc. 2010;93:1437–1442.

[8] Gao Y, Shi C, Ying W. Luminescence properties of SrB_4O_7; Eu, Tb phosphors. Mater Res Bull. 1996;31 (5):439–444.

[9] Dillip GR, Dhoble SJ, Raju BDP. Luminescence properties of $Na_3SrB_5O_{10}:Dy^{3+}$ plate-like microstructures for solid state lighting applications. Opt Mater. 2013;35:2261–2266.

[10] Xu L, Liu C, Guan L, et al. Electrospun nanofibrous mats as skeletons to produce MOF membranes for the detection of explosives. Mater Lett. 2012;87:121–123.

[11] Zhang ZW, Sun X-Y, Liu L, et al. Synthesis and luminescence properties of novel $LiSr_4(BO_3)_3:Dy^{3+}$ phosphors. Ceram Int. 2013;39(2):1723–1728.

[12] Xue Y, Xuewen X, Long H, et al. Synthesis and photoluminescence characteristics of $(Sr, Ca)_3B_2O_6:Eu$ for application in white light-emitting diodes. J Lumin. 2011;131(9):2016–2020.

[13] Wu L, Zhang Y, Chen XL, et al. The $Na_2O–SrO–B_2O_3$ diagram in the B-rich part and the crystal structure of $NaSrB_5O_9$. J Solid State Chem. 2007; 180:1470–1475.

[14] Dillip GR, Ramesh B, Madhukar Reddy C, et al. X-ray analysis and optical studies of Dy^{3+} doped $NaSrB_5O_9$ microstructures for white light generation. J Alloys Compd. 2014;615:719–725.

[15] Dillip GR, Mallikarjuna K, Dhoble SJ, et al. The luminescence and structural characteristics of Eu^{3+} doped $NaSrB_5O_9$ phosphor. J Phys Chem Solids. 2014;75 (1):8–14.

[16] Ramesh B, Devarajulu G, Deva Prasad Raju B, et al. Determination of strain, site occupancy, photoluminescent, and thermoluminescent-trapping parameters of Sm^{3+} doped $NaSrB_5O_9$ microstructures. Ceram Int. 2016;42:1234–1245.

[17] Patil KC. Advanced ceramics: combustion synthesis and properties. Bull Mater. 1993;16(6):533–541.

[18] Hedaoo VP, Bhatkar VB, Omanwar SK. Combustion synthesis and characterization of nanocrystalline alkaline earth aluminate $Sr_4Al_{14}O_{25}:RE(RE = Eu, Dy, Sm)$. Int J Nanosci. 2013;12(4):1350023.

[19] Kim B-J, Hasan Z, Kim J-S. Synthesis and characterization of long persistence $Sr_4Al_{14}O_{25}:Eu^{2+}, Dy^{3+}$ phosphor prepared by combustion method. J Cer Proc Res. 2013;14(5):601–605.

[20] Bajaj NS, Omanwar SK. Tb^{3+} optical transitions in novel luminescence host $NaAlO_2$. J Lumin. 2014;153:288–290.

[21] Awade D Chikte, Omawar SK, Moaril SV. Luminescence properties of red emitting phosphor $NaSrBO_3:Eu^{3+}$ prepared with novel combustion synthesis method. J Lumin. 2013;142:180–183.

[22] Gawande AB, Sonekar RP, Omanwar SK. Synthesis and enhancement of luminescence intensity by co-doping of M+ (M=Li, Na, K) in Ce^{3+} doped strontium haloborate. Opt Mater. 2014;36(7):1143–1145.

[23] Ingle JT, Sonekar RP, Omanwar SK, et al. Combustion synthesis and photoluminescence study of novel red phosphor $(Y_{1-x-y}, Gd_x)BaB_9O_{16}:Eu^{3+}y$ for display and lighting. J Alloys Compd. 2014;608:235–240.

[24] Hedaoo VP, Bhatkar VB, Omanwar SK. $PbCaB_2O_5$ doped with Eu^{3+}: A novel red emitting phosphor. Opt Mater. 2015;45:91–96.

[25] Bhatkar VB, Omanwar SK, Moharil SV. Combustion synthesis of silicate phosphors. Opt Mater. 2007;29 (8):1066–1070.

[26] Lei B, Machida K-I, Horikawa T, et al.. Facile combustion route for low-temperature preparation of Sr_2SiO_4: Eu^{2+} phosphor and its photoluminescence properties, Jpn J Appl Phys. 2010;49:095001.

[27] Hedaoo VP Raikwar, Bhatkar VB, Omanwar SK. Combustion synthesis and photoluminescence in novel red emitting yttrium gadolinium pyrosilicate nanocrystalline phosphor. J Alloys Compds. 2016;672:653–659.

[28] Raikwar VR, Bhatkar VB, Omanwar SK. Facile combustion-derived $LaPO_4:Eu^{3+}$ nanosystem and its photoluminescence properties. Indian J Phys. 2016;90(1):49–56.

[29] Pirees AM, Davolos MR. Luminescence of europium (III) and manganese(II) in barium and zinc orthosilicate. Chem Mater. 2001;13:21–27.

[30] Scherrer P. Bestimmung der Grösse und der inneren Struktur von Kolloidteilchen mittels Röntgensrahlen [Determination of the size and internal structure of colloidal particles using X-rays]. Gottinnger Nachrichten Gesell. 1918;2:98–100.

[31] Patterson A. The scherrer formula for X-ray particle size determination. Phys Rev. 1939;56(10):978–982.

[32] A J C W. X-ray Optics. London: Methuen & Co. Ltd.; 1949.

[33] Williamson GK, Hall WH. X-ray line broadening from filed aluminium and wolfram. Acta Metall. 1953;1:22–31.

[34] Dhananjaya N, Nagabhushana H, Nagabhushana BM, et al. Spherical and rod-like $Gd_2O_3:Eu^{3+}$ nanophosphors—structural and luminescent properties. Bull Mater Sci. 2012;35(4):519–527.

[35] Dillip GR, Dhoble SJ, Raju BDP. Luminescence properties of $Na_3SrB_5O_{10}:Dy^{3+}$ plate-like microstructures for solid state lighting applications. Opt Mater. 2013;35:2261–2266.

[36] Filipe V, Hawe A, Jiskoot W. Critical evaluation of Nanoparticle Tracking Analysis (NTA) by NanoSight for the measurement of nanoparticles and protein aggregates. Pharm Res. 2010;27(5):796–810.

[37] Blasse G. Energy transfer in oxidic phosphors. Phys Lett. 1968;28:444–445.

[38] Dexter DL. A theory of sensitized luminescence in solids. J Chem Phys. 1953;21(5):836–850.

[39] Liu J, Wang XD, Wu ZC, et al. Preparation, characterization and photoluminescence properties of $BaB_2O_4:Eu^{3+}$ red phosphor. Spectrochim Acta A. 2011;79(5):1520–1523.

[40] Yu RJ, Noh HM, Moon BK, et al. Synthesis and luminescence properties of a novel red-emitting phosphor $Ba_3La(PO_4)_3:Eu^{3+}$ for solid-state lighting. J Alloys Compd. 2013;576:236–241.

[41] Radiant imaging color calculator 2.0, Free software for color chromaticity coordinates.